

Adhesion dynamics and durotaxis in migrating cells

Ben Harland¹, Sam Walcott^{1,2} and Sean X Sun^{1,2,3}

¹ Department of Mechanical Engineering, Johns Hopkins University, Baltimore, MD 21218, USA

² Johns Hopkins Physical Sciences in Oncology Center, Johns Hopkins University, Baltimore, MD 21218, USA

³ Whitaker Institute of Biomedical Engineering, Johns Hopkins University, Baltimore, MD 21218, USA

E-mail: ssun@jhu.edu

Received 4 September 2010

Accepted for publication 4 November 2010

Published 7 February 2011

Online at stacks.iop.org/PhysBio/8/015011

Abstract

When tissue cells are plated on a flexible substrate, durotaxis, the directed migration of cells toward mechanically stiff regions, has been observed. Environmental mechanical signals are not only important in cell migration but also seem to influence all aspects of cell differentiation and development, including the metastatic process in cancer cells. Based on a theoretical model suggesting that this mechanosensation has a mechanical basis, we introduce a simple model of a cell by considering the contraction of F-actin bundles containing myosin motors (stress fibers) mediated by the movement of adhesions. We show that, when presented with a linear stiffness gradient, this simple model exhibits durotaxis. Interestingly, since stress fibers do not form on soft surfaces and since adhesion sliding occurs very slowly on hard surfaces, the model predicts that the expected cell velocity reaches a maximum at an intermediate stiffness. This prediction can be experimentally tested. We therefore argue that stiffness-dependent cellular adaptations (mechanosensation) and durotaxis are intimately related and may share a mechanical basis. We therefore identify the essential physical ingredients, which combined with additional biochemical mechanisms can explain durotaxis and mechanosensation in cells.

1. Introduction

Eukaryotic cells explore their environment by extending actin protrusions and forming integrin adhesions with their surroundings [1]. The movement and migration of cells are also powered by a combination of protrusion generation, adhesion formation and cellular contraction [18]. While directed migration of cells is often driven by chemical signals, environmental mechanical signals can also have significant effects [6, 8, 9, 24, 29]. In particular, it has been shown that the elasticity of the substrate (characterized by Young's modulus, E) in contact with the cell can have an influence on the direction of cell migration. This process has been termed durotaxis [2, 23, 27, 28]. The stiffness of the cellular environment is not only important for cell migration but also appears to influence the metastatic process of cancer cells *in vivo* [20, 22, 26, 39]. Therefore, a mechanistic understanding of how environmental mechanical signals influence cellular

movement and cell dynamics is an important question in cell biophysics.

Mechanical properties of the environment not only influence cell migration but also can influence many aspects of the cell life cycle. When cells are plated onto a planar substrate, the morphology and behavior of the cell depends on the stiffness of this substrate [5]. If the substrate is soft, aggregates of adhesion molecules remain small and transitory. In the opposite limit, when the substrate is stiff, a clear network of contractile stress fibers (bundles of F-actin) develops, and strong focal adhesions anchoring the cell to the substrate are seen. Substrate stiffness can also influence the long-term fate of cellular development. It has been shown that differentiation of mesenchymal stem cells to more specialized cells is influenced by the stiffness of the cellular substrate [12, 15, 38]. The mechanisms behind this dependence are complex but appear to involve three basic systems: the actin cytoskeleton, cell-surface adhesions and motor-based contraction. Indeed, a simplified

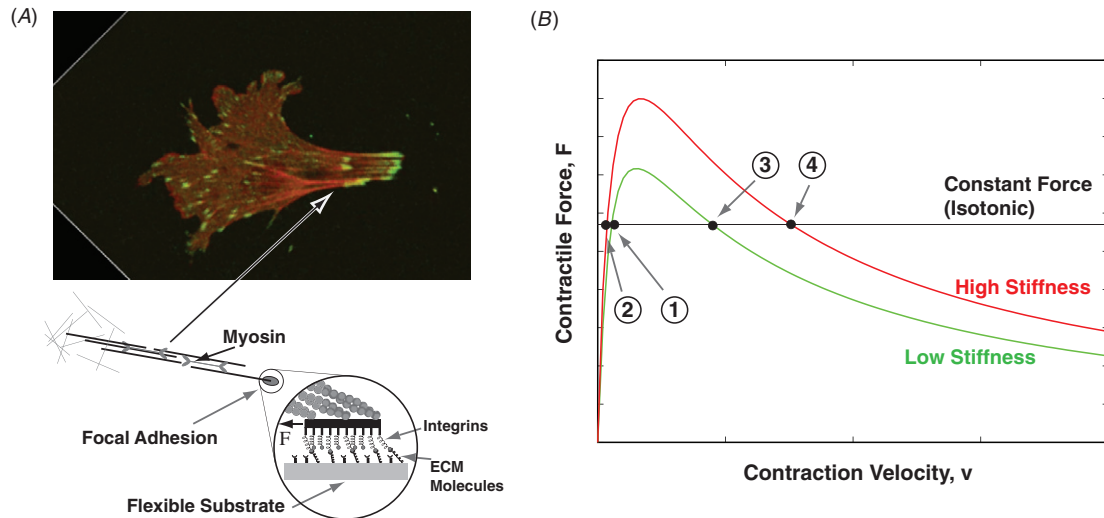


Figure 1. Stress fiber dynamics dominate the movement of tissue cells. (A) A cell on a substrate exhibits a heterogeneous cytoplasm containing a larger number of F-actin bundles (stress fibers) (red bundles), which terminate at integrin focal adhesions (green patches). The sketch shows the mechanical linkages considered in this paper. The stress fibers contain myosin-II, which generates contractile tension along the fiber that pulls on the adhesions. The focal adhesion is a complex of integrins and other regulatory molecules that bind to the extracellular matrix. The ECM molecules are connected to flexible substrates which can deform under mechanical tension (image courtesy of Wirtz Lab, JHU). (B) When stress fibers undergo contraction, focal adhesions provide a drag force that opposes the contraction. The force–velocity curve of adhesion sliding can be obtained from solving equation (1). The full solution is nonlinear and shows two velocities at constant force. At low velocities (points 1,2), higher substrate stiffness results in a lower velocity. At higher velocities (points 3,4), higher substrate stiffness results in a higher velocity. The lower velocity regime might be appropriate for cellular conditions (see the text).

mechanically-based model showed that when the time scales of adhesion movement and the cytoskeleton interaction are considered, cells on stiff substrates will form numerous actin filament bundles with many filaments, while cells on soft substrates will have fewer bundles with a smaller number of filaments [36]. This stiffness-dependent organization of the cellular cytoplasm could be an important feature in cellular mechanosensation.

In this paper, we incorporate this mechanically-based model for mechanosensation into a simple model that describes a cell migrating in response to a substrate stiffness gradient. The cell model adopts the view that the cellular cytoplasm consists of rigid F-actin bundles immersed in a viscous liquid-like background (figure 1). Recent cell mechanics experiments on fibroblasts support this view [17, 37]. Within this model, actin protrusion at the leading edge is a relatively fast process and is mainly for establishing new adhesions. Formation and contraction of the actin bundles (or stress fibers) are relatively slow processes and are responsible for changing the physical location of the cell. Such a view is probably appropriate for tissue cells such as fibroblasts and epithelial cells but is not appropriate for lamellipodium-dominated cells such as keratocytes. We model the formation of adhesions and stress fibers as surface stiffness-dependent stochastic events, and examine the contractile motion of the stress fibers to determine the physical location of the cell. We show that this model exhibits durotaxis. Therefore, it seems that mechanosensation and durotaxis are two aspects of the same cellular processes, and that the stiffness dependence of these processes may have a mechanical basis. Predictions of the model can be experimentally tested.

The organization of the paper is as follows. We describe our cell model of durotaxis in five sections. (i) We review

the physics behind the movement of a focal adhesion under force and discuss the force–velocity (F – V) relationship for this system. (ii) We consider the movement of a single stress fiber on a substrate with a stiffness gradient. (iii) We consider an ensemble of stress fibers behaving according to a few simple rules, thereby forming a minimal cellular durotaxis model (model 1). (iv) We add a model for stiffness-dependent formation of stress fibers to the cellular durotaxis model (model 2). (v) We discuss the simulation scheme used to evaluate durotaxis in these models. Following the description of the model, we show the results of these cellular models moving in a stiffness gradient. We then discuss these results.

2. Model

2.1. Movement of focal adhesions

A crucial element of our model is the adhesion between the cell and the substrate. Such adhesions have been modeled in several different contexts, mostly for adhesions on 2D substrates [6, 7, 24, 25, 30, 36]. A number of results have emerged: by assuming that the adhesions do not grow and the molecular bonds between adhesion molecules are rigid, it is possible to derive the force as a function of velocity for a patch of moving adhesion molecules (figure 1(B)) [31]. This result is semi-analytic and can show the explicit dependence of the F – V curve on the substrate stiffness. The F – V curve shows two different steady states at a given force (figure 1). This model can also exhibit ‘stick-slip’ motion (i.e. an oscillatory steady state). Another entirely different view of adhesion movement postulates that the adhesion patch moves by differential incorporation of new integrin molecules at

different edges of the patch (i.e., treadmilling) [25]. These models of adhesion dynamics await experimental dissection. In this paper, we use the adhesion model of [36], neglecting stick-slip motion, to predict the movement of adhesions on substrates of varying stiffness.

A focal adhesion sliding over a substrate can be modeled by two surfaces that slide relative to one another while cross-linking proteins form transient chemical bonds between them (figure 1). Here, the cross-linkers are integrin molecules that bind to the substrate surface. The cross-linkers have mechanical rigidity, which can be approximated as linear, and are represented by springs in figure 1. These linkers bind to elastic molecules on the substrate surface, which itself has mechanical rigidity. If the top surface, the adhesion, is moving at velocity v relative to the stationary substrate, and the integrin adhesion patch is laterally rigid, then the probability density of the cross-linking protein being bound with molecular strain x at time t ($n(x,t)$) is the solution of the following equation:

$$\frac{\partial n}{\partial t} + v \frac{\partial n}{\partial x} = p_a(x)(1 - N) - k_d(x)n \quad (1)$$

where $k_d(x)$ is the detachment rate as a function of strain, $p_a(x)$ is the attachment rate probability density and the total proportion of attached cross-linkers $N = \int_{-\infty}^{\infty} n(x,t) dx$ [21]. The derivation of this equation assumes that cross-linking molecules are mechanically and chemically independent of each other. The attachment and detachment rate functions ($p_a(x)$ and $k_d(x)$, respectively) can be derived with a minimum number of free parameters (e.g. [10, 11, 13, 35]) that can be experimentally measured. In some cases, these functions can be simplified to provide analytic solutions to equation (1) [31].

We can compute the total force applied on the ECM from the cross-linkers in the focal adhesion from the probability density n through the relation

$$F(t) = N_{ac} \int_{-\infty}^{\infty} \kappa x n(x,t) dx, \quad (2)$$

where κ is the linear stiffness of a single cross-linker and N_{ac} is the total number of integrin cross-linking proteins associated with an adhesion patch. Note that κ is a composite stiffness that includes the stiffness of the integrin cross-linker and ECM, and the substrate elastic modulus [36]. Using a simple linear elastic model, one can show that the composite stiffness is given by

$$\kappa = \frac{CE\bar{\kappa}}{CE + 3\bar{\kappa}} \quad (3)$$

where $\bar{\kappa}$ is the composite spring constant of the integrin–ECM connection. C is the circumference of the assumed circular region over which the integrin molecule exerts force, $C = 2\pi R$, with R being the radius of the circular region. Note that the series stiffness, $\bar{\kappa}$, may involve several molecules connected in series. In the focal adhesion, these molecules include integrins which bind to ECM collagen molecules, and molecules such as vinculin which bind integrins to actin filaments. The value of $\bar{\kappa}$ is dominated by the softest of these molecules.

The full solution of equation (1) can be found for arbitrary sliding velocities if we assume that n is in steady state. From

this steady state solution, the force needed to sustain the sliding velocity can be computed. The resulting F–V curve is shown in figure 1(c). In particular, we show two curves, one for a soft substrate and one for a stiff substrate. At low sliding velocities, the F–V curve is roughly linear, $F \sim bv$, where b is a friction coefficient. Note that b is an increasing function of E , Young’s modulus of the substrate, so that stiffer surfaces will result in a larger friction constant if the force and N_{ac} are equivalent. On the other hand, when the sliding velocity is large, the F–V curve is no longer linear. The dependence of sliding velocity on the substrate stiffness is also reversed. On stiffer substrates, the adhesions slide faster for the equivalent force.

Using realistic molecular parameters and substrate moduli of 1–100 kPa, however, it appears that the high velocity regime does not represent adhesion movement in cells. Typical cell adhesion velocities are around 1–10 nm s^{−1}, and combined with integrin kinetics of ~ 1 s^{−1} [33] the adhesion velocity is slow when compared with molecular dimensions and binding kinetics.

By assuming steady state, we neglect periodic solutions to equation (1). However, under some conditions, oscillatory solutions have been observed [31]. These oscillatory solutions seem to be related to ‘stick-slip’ motion seen in some friction experiments. It has been suggested that stick-slip may be important in cell-surface adhesion sliding (e.g. [7]). The exact details of these oscillations are strongly dependent on the details of the adhesion, such as the number of molecules, the elasticity of the membrane surrounding the adhesion and the inertial and/or viscous properties of the adhesion. Under some choices of these parameters, it has been shown that the relationship between average sliding rate and force can be inverted, whereby adhesions slide faster on stiffer substrates [7]. The stick-slip motion, coupled with the inverted dependence of the slip velocity on substrate elasticity, complicates the movement of adhesions and cells on flexible surfaces. In general, however, in simulations of these stick-slip motions, we find that the steady-state sliding rate is a good approximation to the average sliding rate (simulations not shown). In our models, we neglect this stick-slip adhesion sliding; in section 4, we discuss how stick-slip motion might influence our results.

2.2. Movement of a single stress fiber

Consider a stress fiber of length ℓ connecting two adhesion complexes on a two-dimensional substrate whose Young’s modulus is given by $E(x,y) = \alpha x + \beta$. The stress fiber will exert a force F on each adhesion. The adhesions will then move against the frictional force of the substrate. As discussed in the previous section, if the adhesions move slowly, the F–V relationship for a single adhesion is

$$F = b(E)v, \quad (4)$$

where $b(E)$ is the friction coefficient for the adhesion substrate, neglecting ‘stick-slip’ motion.

The friction coefficient varies with the modulus of the substrate. In [31] an explicit expression for B has been derived:

$$b(E) = N_{ac}\bar{\kappa} \frac{CE}{CE + 3\bar{\kappa}} \frac{k_a}{k_d^0} \left(\frac{1}{k_a + k_d^0} \right). \quad (5)$$

From this expression, we can compute the motion of a contracting stress fiber on a graded substrate. Consider a stress fiber oriented along the x -axis with its center located at the origin. It applies a force of magnitude F to adhesions on each end, and thus the motion of each end (we denote the left adhesion ‘-’ and the one to the right ‘+’) is described by

$$\frac{dx_{\pm}}{dt} = v_{\pm} = \mp \frac{F}{b(E(x_{\pm}, y_{\pm}))}. \quad (6)$$

Note that, for simplicity, we neglect the F–V and force–length relations of the molecular motors generating the force. From this expression, we can compute the center of mass motion (assuming a fiber of uniform density), which is

$$\begin{aligned} \frac{dx_{\text{cm}}}{dt} &= \frac{1}{2} \left(\frac{dx_{-}}{dt} + \frac{dx_{+}}{dt} \right) \\ &= \Lambda(F) \frac{\alpha \ell}{\beta^2} \left(\frac{1}{1 - (\frac{1}{2}\alpha \ell / \beta)^2} \right) \end{aligned} \quad (7)$$

where we have defined

$$\Lambda(F) = \frac{F}{2} \frac{k_a + k_d^0}{N_{ac}} \frac{k_d^0}{k_a} \frac{3\bar{c}}{C}. \quad (8)$$

Thus, we see that on a graded substrate, the center of mass motion of the stress fiber is not zero, instead moving in the direction of higher substrate stiffness. The simple friction model of equation (4) is able to predict the stress fiber velocity as a function of integrin binding/unbinding rates (k_a and k_d^0 , respectively), the size of the adhesions (N_{ac}), the surface Young’s modulus at the stress fiber’s center of mass (β) and the gradient of Young’s modulus (α).

For an ensemble of stress fibers centered at the origin in 1D, if the length of the stress fiber is distributed as $p(\ell)$, then the expected center of mass velocity is

$$\left\langle \frac{dx_{\text{cm}}}{dt} \right\rangle_{\ell} = \Lambda(F) \frac{\alpha}{\beta^2} \int_0^{\infty} d\ell p(\ell) \left[\frac{\ell}{1 - (\frac{1}{2}\alpha \ell / \beta)^2} \right]. \quad (9)$$

For an ensemble of stress fibers in 2D starting with their centers of mass at $x = 0$, we can also compute the center of mass motion as the fibers contract. We must consider an additional coordinate: the orientation of the stress fiber with respect to the x -axis. A fiber of length ℓ applying force F that makes an angle θ with the x -axis has a motion in the x -direction which is the same as that of a fiber of length $\ell \cos \theta$ applying force $F \cos \theta$. Therefore, we have

$$\left\langle \frac{dx_{\text{cm}}}{dt} \right\rangle_{\theta} = \frac{1}{\pi} \int_0^{\pi} d\theta \Lambda \frac{\alpha \ell \cos^2 \theta}{\beta^2} \left[\frac{1}{1 - (\frac{1}{2}\alpha \ell \cos \theta / \beta)^2} \right]. \quad (10)$$

Combined with the previous result with variable ℓ , in the limit where $(\alpha \ell / 2\beta)^2 \ll 1$, the expected velocity approaches

$$\left\langle \frac{dx_{\text{cm}}}{dt} \right\rangle_{\theta, \ell} \approx \Lambda \frac{\alpha \langle \ell \rangle}{2\beta^2} \quad (11)$$

which is half the expected velocity of a fiber oriented along the x -axis.

These results, specifically equations (7) and (11), show that if only contraction of stress fibers is taken into account (neglecting surface stiffness-dependent stress fiber formation),

then the center of mass motion of a collection of stress fibers will exhibit a net movement toward higher stiffness. This model predicts that both the gradient of the stiffness $\alpha = \nabla E(x, y)$ and the nominal stiffness β contribute to the expected migration velocity. The expected velocity increases in proportion to the stiffness gradient but decreases with nominal stiffness squared. These simple predictions can be easily tested in experiments.

Note that here (and in the following sections) we refer to the expectation value of the stress fiber’s (or cell’s) velocity. This value is distinct from the expectation value of the stress fiber’s (or cell’s) speed. For example, a stress fiber undergoing uniform Brownian motion has an expected velocity of zero, yet its expected speed is non-zero.

2.3. Model 1: a friction model for a migrating cell

We consider a migrating cell as a liquid-like cytoplasmic pool containing rigid F-actin contractile bundles (stress fibers). The bundles are randomly oriented, and continuously assemble and disassemble from the cytoplasm. The center of mass of the bundles coincides with the physical location of the cell. One could argue that the cell is located at the position of the nucleus. We assume that the nucleus location is approximately at the center of mass of the bundles because the majority of the stress fibers are perinuclear and connected to the nucleus during contraction [19]. The tension, F , in the stress fiber is assumed to be length and velocity independent and is a free parameter. The stress fibers contract according to the equation of motion

$$F = b_{+}v_{+} = -b_{-}v_{-}, \quad (12)$$

where the subscripts + and – refer to adhesions on opposite ends of the fiber.

New actin protrusions at the cellular periphery are mainly used to establish new adhesion sites. These sites mature and develop into actin stress fiber bundles containing myosin. The contraction of these fibers is relatively slow when compared to protrusion formation.

In this model, which we call model 1, we assume an approximate overall conservation of actin bundle mass. Thus, if a stress fiber contracts to a minimum length: $\ell_{\text{min}} = 200$ nm, then the stress fiber is assumed to disappear, and a new fiber with length ℓ is formed at random orientation and position within radius R_c around the current center of mass of the cell.

2.4. Model 2: including a kinetic description of stress fiber formation

Rather than assuming that actin bundle mass is conserved, we can consider the formation of new stress fibers as stochastic events characterized by one or more rate constants. These rate constants can depend on the local stiffness of the substrate, for example, we might expect that on stiff surfaces the probability of forming bundles is higher than on soft substrates. Therefore, we modify our previous model (model 1) to include the stiffness dependence of stress fiber formation, generating model 2. In this model, we introduce a phenomenological rate density for stress fiber formation, $p_{\text{sf}}(E)$, which determines

the single stiffness-dependent rate constant of stress fiber formation $k_{\text{sf}}(E(x, y))$ in some small area $dA = dx dy$ around point x, y through the relation $k_{\text{sf}}(E) = p_{\text{sf}}(E) dx dy$. The dependence of p_{sf} on E is shown in figure 3.

The rate constant of stress fiber formation, k_{sf} , is determined by the mechanism of stress fiber formation which has been investigated experimentally and theoretically [34, 40, 41]. Experimentally, it is clear that stress fibers are formed preferentially on stiff surfaces. Thus, we have selected a monotonically increasing function that becomes saturated on very stiff surfaces to be qualitatively consistent with this observation. A recent theoretical study argues that cross-linking and bundling between actin filaments and the movement of adhesions are coupled together to generate these actin bundles [36]. The shape of $k_{\text{sf}}(E)$ was selected to be consistent with this theoretical mechanism. Having a single rate constant means that we assume that the fiber formation process is dominated by a single rate-limiting process.

We selected parameters such that the transition between stress fiber-forming and stress fiber-free cells occurs approximately at $E_0 \approx 6$ kPa, and so that a cell on a 6 kPa substrate will have ≈ 30 fibers at equilibrium. This function of course can be adjusted to allow for more or less stress fibers or a different transition stiffness E_0 . Note that $k_{\text{sf}}(E)$ is taken to be twice the rate of formation of stable adhesion complexes, k_{ac} ,

$$k_{\text{sf}}(E(x, y)) = \frac{1}{2} k_{\text{ac}}(E(x, y)) \quad (13)$$

$$k_{\text{ac}}(E) = \left(p_{\text{min}} + \frac{p_{\text{max}} - p_{\text{min}}}{1 + \exp[-\gamma(E - E_0)]} \right) dx dy. \quad (14)$$

It is assumed that pairs of successive adhesions will be joined with a stress fiber. γ is chosen to be 1000 Pa^{-1} , while p_{min} and p_{max} are, respectively, 5×10^{-5} and $5 \times 10^{-4} \text{ s}^{-1} \mu\text{m}^{-2}$.

Given these assumptions, we investigate the overall expectation value of the velocity of an ensemble of cells for these two simple models. In model 1, the fiber dynamics are only governed by differential drag of the focal adhesions, and the number of stress fibers is held fixed, regardless of substrate stiffness. In model 2, the fiber movement is treated as in model 1, but the rate of appearance of fibers is determined by k_{sf} . Therefore, the steady-state number of fibers in the cell is also a function of the substrate stiffness. The parameters used in the models are estimated from typical molecular values, and are summarized in table 1.

2.5. Simulation scheme

The goal of the simulations is to determine the dependence of the expected cell migration velocity on two substrate parameters: (i) cell stiffness, characterized by Young's modulus, $E = \beta$, and (ii) the stiffness gradient, $\nabla E = \alpha$. Therefore, for a circular cell of radius R_c on a 2D substrate, the value of $E(x, y)$ at any point within the cellular boundary ($\sqrt{x^2 + y^2} < R_c$) is given by $E(x, y) = \alpha x + \beta$, assuming that the origin is at the cell center. The general setup for the simulations is as follows.

Table 1. Parameters used and their values in the models. These parameters are estimated from typical molecular properties. Our results only depend weakly on the exact values of the parameters.

Parameter	Description	Value	Units
$\bar{\kappa}$	Composite stiffness of adhesion-ECM molecule	25	pN nm ⁻¹
R	Radius of a single ECM molecule	1	nm
k_a^0	Unstrained binding rate of AC-ECM	1	s ⁻¹
k_d^0	Unstrained off rate of AC-ECM	1	s ⁻¹
N_{ac}	Number of adhesion molecules per complex	10 ³	–
R_c	Cell radius	20	μm
N_{sf}	Number of stress fibers	30	–
E	Young's modulus of substrate	10 ² –10 ⁴	Pa
F	Tensile force of SF	500	pN

- (i) A starting configuration is generated in which a desired number of stress fibers are arranged within a circle of radius R_c centered at the origin (the cell membrane) such that the endpoints of each stress fiber are positioned according to a uniform distribution.
- (ii) An equilibration period (200 s) simulation is carried out by integrating the equation of motion (equation (12)) in order to obtain a starting number and arrangement of stress fibers. As the individual fibers move, so does their collective center of mass. The center of the cell membrane (the circle of radius R_c into which new fibers are added) moves with the stress fiber center of mass (figure 2(a)).
- (iii) The cell and the collection of stress fibers are repositioned so that they are again centered at the origin, and the cell is allowed to move over a short period (50 seconds) and its position is measured (figure 2(B)).
- (iv) Steps 1–3 are performed until the averaged cellular velocities have converged to the expected cell velocity (figure 2(B)).

In the case of model 2, the Gillespie algorithm [16, 32] is used. The times at which mature stress fibers appear in our model cell are sampled from the distribution

$$p(t) = e^{-Kt}, \quad (15)$$

where K is the escape rate for a cell with any particular number of stress fibers, N_{sf} ,

$$K = \int_{\text{cell}} dx dy p_{\text{sf}}(E(x, y)). \quad (16)$$

During a simulation, when these stochastic timepoints are encountered, a new fiber is introduced with the adhesions placed at a position (x, y) within R_{cell} of the cell center according to the probability

$$p_{\text{ac}}(x, y) = \frac{1}{K} p_{\text{ac}}(E(x, y)). \quad (17)$$

In the absence of a stiffness gradient, the rate of fiber addition is determined by the constant K which is independent of cell position. Therefore, although individual cells perform random walks, net cell movement will not occur and $N_{\text{sf}} \sim K(E)$ will have a well-defined steady-state value (see figure 3).

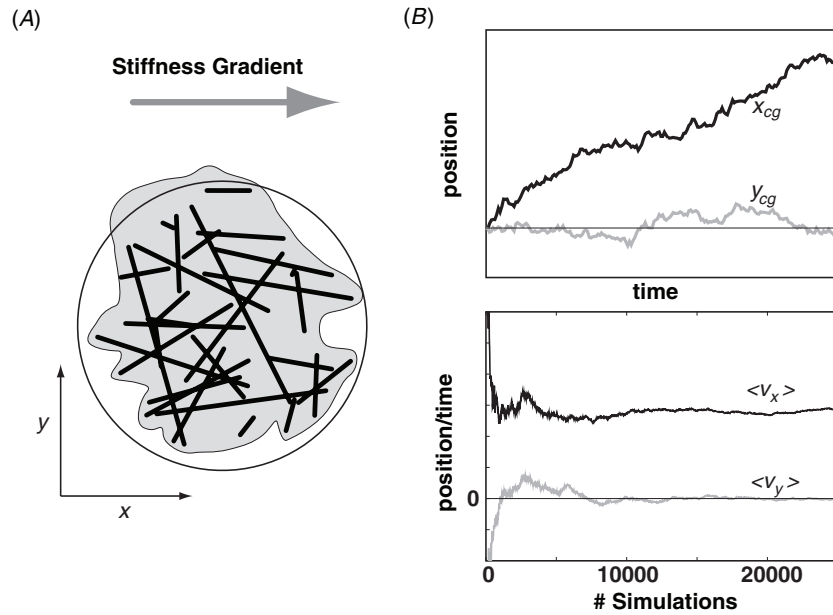


Figure 2. Simple model of the migrating cell considered in this paper. (A) The cell is a collection of stress fibers undergoing contraction and birth/death process. The creation of stress fibers is stochastic and centered at the center of mass of the cell. The rate of fiber creation can depend on the local substrate stiffness. The contraction of the fiber is governed by equation (12). (B) This simple model shows durotaxis if there is a substrate stiffness gradient in the x -direction. The average cell position moves toward higher stiffness (upper plot). The expected velocities in the x - and y -directions are obtained by averaging over many simulations (lower plot).

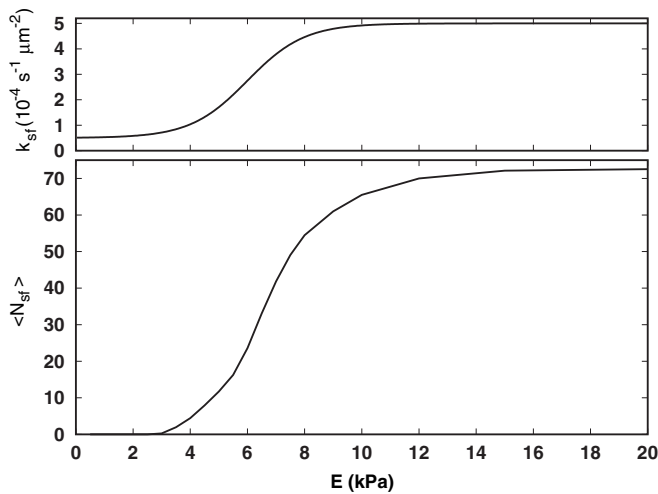


Figure 3. Results for cell model 2 based on both stress fiber addition kinetics and stiffness-dependent drag coefficients. This plot shows that (to zeroth order) the number of stress fibers in our cell model depends on the addition rate for adhesion complexes. The rate constant, k_{sf} , is an addition rate *density* per cell area. Below 3 kPa, stress fibers disappear more rapidly than they form, and during equilibration, all the stress fibers are lost and durotaxis is not possible.

3. Simulation results

For both models, individual trajectories obtained from the simulations of the model cell in the absence of a stiffness gradient exhibit motility in the form of a cellular random walk with zero expected velocity ($\langle v \rangle = 0$ but non-zero speed $\langle v^2 \rangle > 0$). When a stiffness gradient is introduced in the

x -direction, there is a positive expected velocity, $\langle v_x \rangle$, while the y -component, $\langle v_y \rangle$, remains zero.

The dependence of the simulated cell migration expected velocity on the substrate parameters E and ∇E is shown in figure 4 for model 1. As predicted by equation (7), this expected velocity is proportional to the stiffness gradient and inversely proportional to the square of Young's modulus. The proportionality constant in the case of the single stress fiber (figure 4, bottom) is $0.68 \text{ kPa } \mu\text{m}^2 \text{ s}^{-1}$, in agreement with equation (10) when equation (10) is integrated numerically using the expected value for the stress fiber length, $\langle \ell \rangle$.

When model 2 is studied, more complex and interesting behavior emerges. Again, when there is no gradient, there is no net migration. The average number of stress fibers in the cell, however, now depends on the stiffness of the substrate. This is in accord with experimental observations of cells on varying substrates: on soft surfaces, the cytoplasm is generally diffuse and devoid of stress fibers, and on stiff surfaces, a larger number of fibers and bundles are seen.

When a stiffness gradient is introduced in model 2, net migration occurs. Figure 5, bottom, shows the relationship between the expected migration velocity and E . First, cells on a substrate below certain threshold, $E \approx 2.5 \text{ kPa}$, have zero stress fibers at steady state and therefore are not observed to undergo durotaxis. Above this threshold, the shapes of the $\langle v \rangle$ curves are observed to be a combination of four features:

- (i) As observed in model 1 based on differential drag, $\langle v \rangle \propto \nabla E$.
- (ii) Also as before, at large E 's, expected velocities fall off as $1/E^2$.
- (iii) At intermediate stiffness, $E \sim 6 \text{ kPa}$, the expected velocities are roughly proportional to the gradient of the

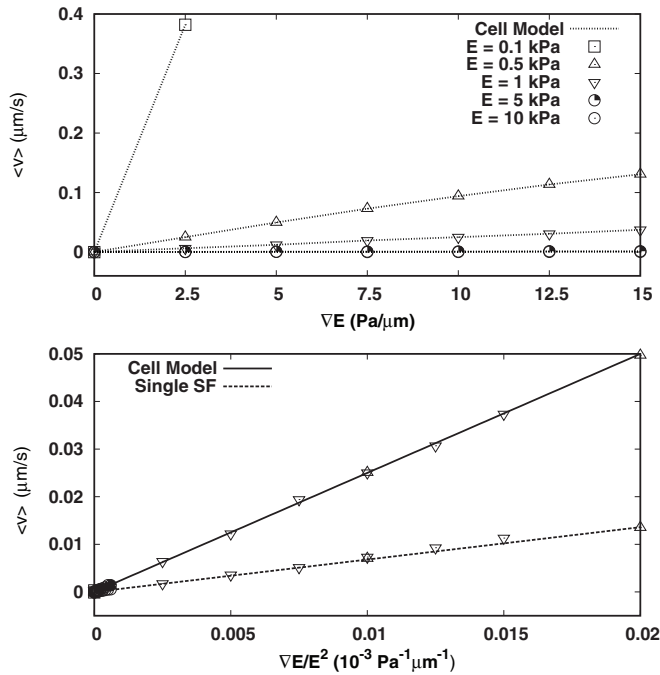


Figure 4. Results for our cell model based on stress fiber differential drag (model 1). The velocity of cell migration is proportional to the substrate stiffness gradient and inversely proportional to the square of Young's modulus. The results show that the cell moves faster as the substrate gradient is increased but moves slower as the background stiffness is increased.

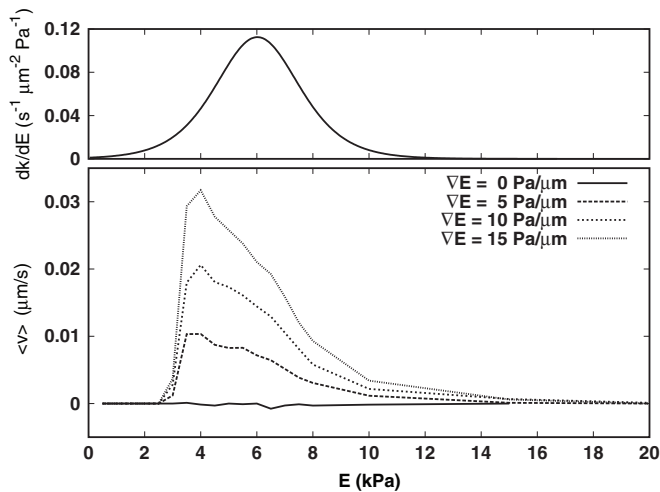


Figure 5. Results for cell model 2 based on both stress fiber addition kinetics and stiffness-dependent drag coefficients. The migration velocity of the cell depends upon three factors. 1. Migration is enhanced in regions where E coincides with a large gradient in $k_{sf}(E)$ (top panel) and not supported when E is below some threshold value. 2. Larger migration velocities are observed for large E gradients. This relationship is linear as observed in the previous model.

rate constant, dk_{ac}/dE . It is this quantity which biases the position of the newly formed stress fibers. Because we have defined the center of the cell as the center of mass position of the existing stress fibers, the addition of new fibers provides an additional contribution to the net

direction of cell migration. In fact, when simulations are carried out in which the drag coefficient, B , is independent of E , the $\langle v \rangle$ - E curves bear the same shape as dk_{ac}/dE .

- (iv) For most stiffness gradients, there is an optimal stiffness where the expected migration velocity is the highest. This result can be explained by the fact that at low stiffnesses, the cell does not have significant number of stress fibers and therefore does not move. At high stiffnesses, the net drag on the adhesions is too high, and the cell also does not move quickly. Thus, it is at intermediate stiffnesses, where stress fibers form yet adhesion drag is not too high, that maximum durotaxis speed occurs.

Therefore, we conclude that the dependence of $\langle v \rangle$ on ∇E contains (additive) contributions from both the differential slippage of section 2.2 and the gradient of the rate constant (which is also a consequence of ∇E).

When these results are taken together, we see that model 2 seems to be broadly consistent with experimental observations: cells on soft substrates do not form a significant number of stress fibers; cells on very stiff surfaces have a larger number of fibers. Further, the model makes predictions that can be experimentally tested, for example, that only at intermediate stiffnesses do cells move toward regions of high stiffness. Our model also makes specific predictions on the dependence of the expected migration velocity on the absolute value of the substrate modulus as well as the gradient of the modulus. Experimental tests of these predictions would help shed light on the details of both mechanosensation and durotaxis.

4. Conclusions and discussion

A detailed understanding of the mechanisms of cell mechanosensation and durotaxis is an important and pressing problem in cell biophysics, as mechanosensation and durotaxis have been implicated in such medically-relevant processes as stem cell lineage determination and cancer metastasis, respectively. Recent theoretical work suggests that mechanosensation may have a mechanical basis. In particular, the stiffness-dependent sliding of focal adhesions can lead to stiffness-dependent forces on the cytoskeleton that then result in different steady-state numbers of stress fibers, replicating the experimental observation that stress fibers form preferentially on stiff surfaces [36].

Here, we introduce a cellular model of durotaxis based on formation and contraction of actin stress fiber bundles. This cellular model relates the dynamics of subcellular structures to the expected migration velocity of the cell. Using the adhesion model that predicts faster sliding on soft surfaces, differential substrate stiffness at the two ends of a stress fiber results in a net movement of the fiber toward a stiffer substrate. We are therefore able to show that differential drag alone is sufficient to result in durotaxis in a cell (model 1). In order to replicate the stiffness-dependent formation of stress fibers, we introduce a kinetic model of stress fiber formation and couple this model to the contraction dynamics (model 2). This model shows a range of behaviors that are reasonable. Therefore, it seems that mechanosensation and durotaxis are simply two manifestations of the same stiffness-dependent

cellular adaptations, and that these adaptations may have a mechanical basis.

Absent from this model is a coupling between the direction of cell migration and stress fiber alignment, or cell shape (e.g. [41]). Including a mechanism for stress fibers to align with the direction of cell movement will increase the rate of durotaxis. Equation (10) provides a relationship for stress fiber orientation and expected velocity. Such orientation effects would have a small influence on our qualitative results but might tend to bias the maximum durotaxis rate toward stiffer surfaces (i.e. provide a rightward shift of the peaks in figure 5). Allowing cell shape to change as a function of time or stress fiber position would also affect the model, whereby if the cell's dimensions were increased along the stiffness gradient, the cell would move faster. Again, if cells tend to extend along the stiffness gradient in a stiffness-dependent fashion, we would see a rightward shift of the peaks in figure 5.

The model makes specific predictions on the dependence of the expected migration velocity as a function of substrate stiffness gradient, ∇E , and the absolute value of the substrate stiffness. Perhaps the simplest prediction of the model is that durotaxis does not occur either on very stiff or very soft surfaces, where in the former case, an insufficient number of stress fibers form to power movement, and in the latter case adhesion sliding ceases to be stiffness dependent (i.e. equation (5) becomes constant at large E).

Another experiment could determine the relative contribution of adhesion sliding to stiffness-dependent stress fiber formation, and could provide insight into the effect of substrate stiffness on adhesion dynamics. In particular, our model predicts that in the absence of stiffness-dependent adhesion sliding, the maximum expected durotaxis rate occurs when the slope of the stress fiber formation rate versus stiffness plot is maximized. When stiffness-dependent sliding is included in the model, the maximum durotaxis rate shifts to softer surfaces, as adhesion sliding is fastest on these surfaces. Thus, simultaneous measurement of the probability of stress fiber formation and durotaxis as a function of surface stiffness could determine the relative contribution of these two effects. If, as suggested by some models, adhesions slide more slowly on soft surfaces, then the maximum durotaxis rate should shift to stiffer surfaces. Different models of adhesion sliding are discussed in more detail in the next section.

If these experiments support the predictions of our model, additional experiments could further probe details of the model. For example, the model shows that an important factor that can influence the net migration of the cell on a graded substrate is the rate of formation of F-actin stress fibers. In an earlier work, two of us showed that the rate of fiber formation depends on the cross-linking dynamics of actin filaments and the rate of actin filament turnover in the cytoplasm [36]. By manipulating these factors, it is possible to influence the fiber formation process, which would ultimately influence cell migration speed. For example, by increasing the number of stress fibers, perhaps by over-expressing a cross-linker, it might be possible to induce durotaxis on surfaces that are too soft to support durotaxis in wild-type cells.

4.1. Stick-slip and treadmilling

The model we used to describe the adhesion movement is relatively simple, neglecting oscillatory steady states that have been identified with stick-slip motion. It has been argued that stick-slip-like motion is important in adhesion sliding [3, 7]. Interestingly, these models can show an inversion of the stiffness-dependent adhesion sliding used here, where stick-slip can cause adhesions to slide fastest on soft surfaces [7]. In this case, our model that neglects stiffness-dependent adhesion formation (model 1) predicts that cells should migrate toward softer surfaces—reverse durotaxis. In order to observe durotaxis, stiffness-dependent stress fiber formation would have to more than compensate for this effect. Intriguingly, this antagonistic effect between adhesion sliding and stress fiber formation could result in a situation where cells migrate toward a particular stiffness—that is, on stiff surfaces cells would exhibit reverse durotaxis, while on soft surfaces they would exhibit durotaxis.

Besides these models of friction-like sliding of adhesions, some experimentalists and theorists have argued for treadmilling of adhesions, where adhesion motion is accomplished by adding new molecules preferentially to the side in the direction of force and removing them from the opposite side [24]. While the surface stiffness dependence of this process is somewhat unclear, our model suggests that as long as sliding rate decreases with increasing surface stiffness, this mechanism could result in cell durotaxis. If the opposite is true, and sliding rate increases with surface stiffness, then stiffness-dependent adhesion formation would need to compensate for the reverse durotaxis effect of adhesion sliding. Detailed experiments on adhesions have yet to determine which, if any, of these adhesion models is correct; however, a recent experiment seems to support frictional sliding rather than treadmilling [3].

4.2. Durotaxis in 3D

The present model is best applied to cells on 2D substrates, such as epithelial cells. For other tissue cells *in vivo*, a number of features are significantly different [4, 14]. For example, large focal adhesions do not seem to form in cells in a 3D matrix [14], although adhesions to collagen fibers must be present for cells to adhere in 3D. The actin cytoskeleton also seems to be organized differently in 3D. Nevertheless, contractile forces in the cytoskeleton and adhesion movement must also play roles in 3D durotaxis and cell motility. Some of the modeling concepts in the present paper can be extended to the 3D environment. Further studies on cell movement in 3D may reveal the role of matrix stiffness directing cell migration.

4.3. Conclusions

Using two observations derived from a mechanically-based model for mechanosensation, i.e. that adhesions slide more slowly and that stress fibers form most readily on stiff surfaces, we have shown that cells that exhibit these properties also exhibit durotaxis, directed migration toward surfaces of higher stiffness. Thus, we are able to demonstrate that

mechanosensation and durotaxis may be explained by the same basic processes, which may have a mechanical, as opposed to a biochemical, basis. Our durotaxis model connects subcellular and molecular properties to properties at the whole cell level, while still retaining sufficient simplicity to allow analytic calculations to predict its behavior in some limiting cases. The model also makes a variety of predictions that can be experimentally tested, for example, that durotaxis should be observed only at intermediate stiffnesses. By carrying out these experiments, various details of the model may be revised, leading to a deeper understanding of both durotaxis and mechanosensation.

Acknowledgments

The authors would like to thank Denis Wirtz for useful discussions. The work has been supported by NSF CHE0514749, NIH GM075305 and NIH 1U54CA143868.

References

- [1] Alberts B, Johnson A, Lewis J, Raff M, Roberts K and Walter P 2002 *Molecular Biology of the Cell* 4th edn (New York: Garland Science)
- [2] Allieux-Guerin M, Icard-Arcizet D, Durieux C, Henon S, Gallet F, Mevel J, Masse M, Tramier M and Coppey-Moisan M 2009 Spatiotemporal analysis of cell response to a rigidity gradient: a quantitative study using multiple optical tweezers *Biophys. J.* **96** 238
- [3] Aratyn-Schaus Y and Gardel M L 2010 Transient frictional slip between integrin and the ECM in focal adhesions under myosin II tension *Curr. Biol.* **20** 1145
- [4] Bloom R, Celedon A, Sun S X and Wirtz D 2008 Mapping local matrix remodeling induced by a migrating tumor cell using 3-d multiple particle tracking *Biophys. J.* **95** 4007
- [5] Brown A E X and Discher D E 2009 Conformational changes in cell and matrix physics *Curr. Biol.* **19** R781
- [6] Bruinsma R 2005 Theory of force regulation by nascent adhesion sites *Biophys. J.* **89** 87
- [7] Chan C E and Odde D J 2008 Traction dynamics of filopodia on compliant substrates *Science* **322** 1687
- [8] Chen C S 2008 Mechanotransduction - a field pulling together? *J. Cell Sci.* **121** 3285
- [9] DeMali K A, Wennerberg K and Burridge K 2003 Integrin signaling to the actin cytoskeleton *Curr. Opin. Cell Biol.* **15** 572
- [10] Dudko O K, Filipov A E, Klafter J and Urbakh M 2003 Beyond the conventional description of dynamic force spectroscopy of adhesion bonds *Proc. Natl Acad. Sci.* **100** 11378
- [11] Dudko O K, Hummer G and Szabo A 2006 Intrinsic rates and activation free energies from single-molecule pulling experiments *Phys. Rev. Lett.* **96** 108101
- [12] Engler A J, Griffin M A, Sen S, Bonnemann C G, Sweeney H L and Discher D E 2004 Myotubes differentiate optimally on substrates with tissue-like stiffness: pathological implications for soft or stiff microenvironments *J. Cell Biol.* **166** 877
- [13] Evans E 2001 Probing the relation between force-lifetime-and chemistry in single molecular bonds *Ann. Rev. Biophys. Biomol. Struct.* **30** 105
- [14] Fraley S, Feng Y, Kim D H, Celedon A, Longmore G D and Wirtz D 2010 The distinct role of focal adhesion proteins in three dimensional cell motility *Nat. Cell Biol.* **12** 598
- [15] Georges P C and Janmey P A 2005 Cell type-specific response to growth on soft materials *J. Appl. Physiol.* **98** 1547
- [16] Gillespie D T 1977 Exact stochastic simulation of coupled chemical reactions *J. Phys. Chem.* **81** 2340
- [17] Hale C M, Sun S X and Wirtz D 2009 Resolving the role of actomyosin contractility in cell microrheology *PLoS One* **16** e7054
- [18] Heidemann S R and Buxbaum R E 1998 Cell crawling: first the motor, now the transmission *J. Cell Biol.* **141** 1
- [19] Khatau S B, Hale C M, Stewart-Hutchinson P J, Patel M S, Stewart C L, Searson P C, Hodzic D and Wirtz D 2009 A perinuclear actin cap regulates nuclear shape *Proc. Natl Acad. Sci.* **106** 19017
- [20] Kumar S and Weaver V M 2009 Mechanics, malignancy and metastasis: the force journey of a tumor cell *Cancer Metastasis Rev.* **28** 113
- [21] Lacker H M and Peskin C S 1986 A mathematical method for the unique determination of cross-bridge properties from steady-state mechanical and energetic experiments on macroscopic muscle *Lect. Math. Life Sci.* **16** 121
- [22] Levental K R *et al* 2009 Matrix crosslinking forces tumor progression by enhancing integrin signaling *Cell* **139** 891
- [23] Lo C, Wang H, Dembo M and Wang Y 2000 Cell movement is guided by the rigidity of the substrate *Biophys. J.* **79** 144
- [24] Nicolas A, Geiger B and Safran S A 2004 Cell mechanosensitivity controls the anisotropy of focal adhesions *Proc. Natl Acad. Sci.* **101** 12520
- [25] Nicolas A, Besser A and Safran S A 2008 Dynamics of cellular focal adhesions on deformable substrates: consequences for cell force microscopy *Biophys. J.* **95** 527
- [26] Paszek M J and Weaver V M 2004 The tension mounts: mechanics meets morphogenesis and malignancy *J. Mammary Gland Biol. Neoplasia* **9** 325
- [27] Pelham R J and Wang Y 1997 Cell locomotion and focal adhesions are regulated by substrate flexibility *Proc. Natl Acad. Sci.* **94** 13661
- [28] Pelham R J and Wang Y 1998 Cell locomotion and focal adhesions are regulated by the mechanical properties of the substrate *Biol. Bull.* **194** 348
- [29] Peschetola V, Verdier C, Duperray A and Ambrosi D 2009 Cancer cell migration on 2d deformable substrates *Cell Mechanics: From Single Scale-Based Models to Multiscale Modeling* ed A Chauviere, L Preziosi and C Verdier (Boca Raton, FL: CRC Press) pp 243–63
- [30] Shemesh T, Geiger B, Bershadsky A D and Kozlov M M 2005 Focal adhesions as mechanosensors: a physical mechanism *Proc. Natl Acad. Sci.* **102** 12383
- [31] Srinivasan M and Walcott S 2009 Binding site models of friction due to the formation and rupture of bonds: state-function formalism, force-velocity relations, response to slip velocity transients, and slip stability *Phys. Rev. E* **80** 046124
- [32] Sun S X, Lan G and Atilgan E 2008 Stochastic simulation methods in cell biology *Methods Cell Biol.* **89** 601
- [33] Taubenberger A *et al* 2007 Revealing early steps of $\alpha_2\beta_1$ integrin-mediated adhesion to collagen type I using single-cell force spectroscopy *Mol. Biol. Cell* **18** 1634
- [34] Theyry M, Pepin A, Dressaire E, Chen Y and environment M Bornens Cell distribution of stress fibres in response to the geometry of the adhesive 2006 *Cell Motil. Cytoskeleton* **63** 341
- [35] Walcott S 2008 The load dependence of rate constants *J. Chem. Phys.* **128** 215101
- [36] Walcott S and Sun S X 2010 A mechanical model of actin stress fiber formation and substrate elasticity sensing in adherent cells *Proc. Natl Acad. Sci.* **107** 7757

- [37] Wirtz D 2009 Particle-tracking microrheology of living cells: principles and applications *Ann. Rev. Biophys.* **38** 301
- [38] Yeung T, Georges P C, Flanagan L A, Marg B, Ortiz M, Funaki M, Zahir N, Ming W, Weaver V and Janmey P A 2005 Effects of substrate stiffness on cell morphology, cytoskeletal structure, and adhesion *Cell Motil. Cytoskeleton* **60** 24
- [39] Zaman M H, Trapani L M, Sieminski A, Walls A, Lauffenburger D A and Matsudaira P T 2006 Migration of tumor cells in 3d matrices is governed by matrix stiffness along with cell-matrix adhesion and proteolysis *Proc. Natl Acad. Sci.* **103** 10889
- [40] Zemel A, Rehfeldt F, Brown A E X, Discher D E and Safran S A 2010a Cell shape, spreading symmetry, and the polarization of stress-fibers in cells *J. Phys.: Condens. Matter* **22** 1
- [41] Zemel A, Rehfeldt F, Brown A E X, Discher D E and Safran S A 2010b Optimal matrix rigidity for stress-fibre polarization in stem cells *Nat. Phys.* **6** 468